Comparative study between different frequency strategies for relative dielectric permittivity and electrical conductivity reconstruction. Application to near subsurface imaging

Quentin Didier, Slimane Arhab, Gaëlle Lefeuve-Mesgouez

Comparative study between different frequency strategies for relative dielectric permittivity and electrical conductivity reconstruction. Application to near subsurface imaging

Quentin Didier, Slimane Arhab and Gaëlle Lefeuve-Mesgouez

UMR 1114 EMMAH, Avignon Université – INRAE, F-84914 Avignon, France

***Abstract*—This work proposes a comparative study between different frequency strategies for the simultaneous reconstruction of the relative dielectric permittivity and electrical conductivity of the near subsurface. Data on the electric field are generated in the framework of a ground penetrating radar (GPR) configuration. Assessing these two parameters from the data requires solving a nonlinear and ill-posed inverse problem, which is solved iteratively by a regularized Gauss-Newton (RGN) algorithm. Numerical results allow to determine an optimal strategy, for which convergence rate and computation time are reasonable, spatial resolution is improved and the two parameters are very well reconstructed.**

***Index Terms*—ground penetrating radar, full waveform inversion, frequency domain, regularized Gauss-Newton, finite-element method, bi-parameter reconstruction.**

I. Introduction

GPR aims to reconstruct the relative dielectric permittivity and electrical conductivity of an heterogeneous subsurface. The physical configuration consists of an incident wave radiated by a transmitter positioned above the air/ground interface [1]. This wave interacts with the interface and the heterogeneities of the subsurface. The resulting electromagnetic field is measured at a receiver also positioned above the air/ground interface but laterally offset from the transmitter.

From the knowledge of the excitation and the measurements at several receivers, the aim is to establish as well as possible a mapping of the electromagnetic properties of the investigated medium. This requires an efficient forward model and an associated inversion strategy. This paper focuses on the second one. There are different methods to exploit the data in order to find the electromagnetic parameters of the medium: we can mention in particular the global [2] or local [3] optimization methods and the methods resulting from the recent development of deep-learning [4]. However, the approaches related to deep-learning and global optimization are not really adapted to our goal. Indeed, the deep-learning ones require a simple representation of the medium to be reconstructed, and a training phase that is costly in terms of computing time and resources. In the same way, the global optimization is suitable when there are only few unknowns. Among the local optimization methods, full waveform inversion (FWI) is of major interest for the case under consideration. Although initially developed in the 80's [5], FWI has known a huge development relatively recently, namely since the 2010's with the multi-parameter inversion [6], mainly due to the fast increase in processing and storage capacities of computers. Compared to other approaches, FWI is not costly in terms of computing time and in memory resources which is a great advantage. By exploiting all the information embedded in the data, FWI allows to get a fine reconstruction of the ground without knowing a priori neither the shape nor the parameters of the burried objects. Obviously, it is still needed to have an initial guess of the reconstructed medium.

FWI can be formulated equivalently in temporal and frequency regimes. We choose the second one which allows to better handle the data according to their frequencies. Moreover, it can be applied to both frequency and temporal data after being Fourier transformed. Inverting GPR data is a non linear and ill-posed inverse problem. In this case the data show an identical sensitivity with respect to the relative dielectric permittivity and the electrical conductivity, so it is difficult to separate these two parameters in the inversion process. However, these difficulties can be solved by local optimization approaches such as the Quasi-Newton (L-BFGS) [6]–[8] and the regularized Gauss-Newton (RGN) methods. In this work we select the RGN algorithm, because it is accurate, simple to implement and yields a reasonable RAM management [9]. There are different ways to use the data according to their frequencies in the inversion process, which we refer to as "strategies". The contribution of this work is twofold: firstly, to show the ability of RGN algorithm for multi-parameter reconstruction; secondly, to compare four strategies using frequency data in different ways, and then to discuss the strengths and weaknesses of each one in order to define an optimal one.

This paper is organized as follows: after this introduction, the study configuration and the forward model are presented in Section II. Section III is devoted to the description of the inversion process. The numerical results are shown and discussed in Section IV. Finally, the conclusion is given in

Section V.

II. Study configuration and forward model

A. Forward model

In a fixed Cartesian coordinate system (O,**x**,**y**,**z**), a two-dimensional medium with an invariance axis along O**z** is considered, as shown in Fig. 1. The medium is heterogeneous in the $\mathcal{S}$ domain and homogeneous around it. It is described by its relative dielectric permittivity $\varepsilon_r(\mathbf{r})$ and its electrical conductivity $\sigma(\mathbf{r})$, which depend on the spatial position $\mathbf{r} = x\,\mathbf{x} + y\,\mathbf{y}$ (x and y spanning the entire $\mathcal{S}$ domain). As justified in [7] and [8], we assume them to be frequency independent in the frequency range of GPR. We consider an harmonic time dependence for the electric field. The transmitter that radiates the incident wave at the ω_k frequency is modeled by a source term $\mathbf{J}_m^k\,\delta(\mathbf{r}-\mathbf{r}_m) = J_m\,e^{-\mathrm{j}\,\omega_k\,t}\,\delta(\mathbf{r}-\mathbf{r}_m)\,\mathbf{z}$ of amplitude $J_m = 1$ oriented along O**z** axis and positioned at point $\mathbf{r}_m = x_m\,\mathbf{x} + y_m\,\mathbf{y}$, with j the imaginary number such that $\mathrm{j}^2 = -1$. Here δ corresponds to the Dirac delta function. These assumptions situate our study in the context of a TE polarization configuration, which corresponds to an electric field oriented along the invariance axis. In this case we write $\mathbf{E}(\mathbf{r}) = E(\mathbf{r})\mathbf{z}$, reducing the electric field to its scalar component $E(\mathbf{r})$, which satisfies the following scalar Helmholtz equation [10]:

$$\Delta E(\mathbf{r}) + \frac{\omega_k^2}{c_0^2}\left[\varepsilon_r(\mathbf{r}) - \mathrm{j}\frac{\sigma(\mathbf{r})}{\varepsilon_0\,\omega_k}\right] E(\mathbf{r}) = -\mathrm{j}\,\omega_k\,J_m\,\delta(\mathbf{r}-\mathbf{r}_m) \tag{1}$$

with $c_0 = \dfrac{1}{\sqrt{\varepsilon_0\mu_0}}$ the speed of light in vacuum and Δ the Laplacian operator. The solution $E(\mathbf{r}) = E(\mathbf{r},\mathbf{r}_m,\omega_k)$ calculated at point **r** depends implicitly on the position $\mathbf{r}_m$ and the frequency ω_k of the source term. Here, (1) is solved by the finite element method with the module *Wave Optics* of the commercial software *Comsol Multiphysics*®.

B. Study configuration

Fig. 1 illustrates the specific configuration under study: the light grey area corresponds to the heterogeneous zone which extends over a 5 m wide and 4 m deep rectangle. The outer homogeneous part uses PMLs to avoid reflections at the boundaries of the domain. The data employed for the near surface reconstruction are generated from the same software as the forward model used for the inversion. However, to avoid as much as possible the inverse crime [11], a different meshes are involved: one for the inversion process and one for reference data. A white Gaussian noise is added to the latter with a signal to noise ratio of 30. The sources are placed above the surface at 25 cm from the ground and the common mid-point and common offset acquisition modes are retained for the measurements. Twelve transceivers are used, since a transceiver cannot radiate and detect at the same time ($l \neq m$) and due to reciprocity theorem, they lead to 66 separate measurements per frequency.

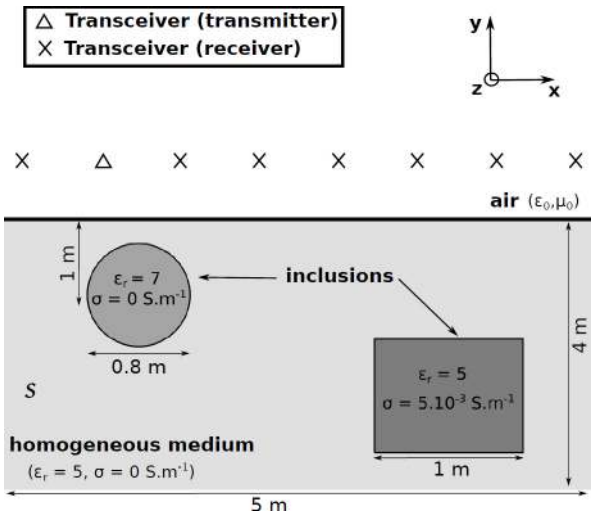

Fig. 1. Configuration of the numerical study

The actual medium to be reconstructed is composed of two inclusions, one being a circle of permittivity 7 and zero conductivity and the other being a square of conductivity $5\cdot10^{-3}\ S.m^{-1}$ and permittivity 5, see Fig. 1. The medium surrounding these two inclusions has a permittivity of 5 and a nul conductivity. This study configuration is interesting to demonstrate the ability of the inversion algorithm to avoid the so-called "trade-off" between the parameters, and then to reconstruct the conductivity and permittivity distinctly with a good spatial resolution.

III. Inversion scheme and frequency startegies

A. Inversion scheme

At each step n of the regularized Gauss-Newton iterative scheme, corrections on the parameters are calculated in order to minimize a cost function defined as follows:

$$\mathcal{F}_n = \frac{\sum\limits_{\substack{\omega_k\\ \in\Omega}}\sum\limits_{\substack{l=1\\ l\neq m}}^{N_S}\sum\limits_{m=1}^{N_S} |E^{obs}(\mathbf{r}_l,\mathbf{r}_m,\omega_k) - E^n(\mathbf{r}_l,\mathbf{r}_m,\omega_k)|^2}{||E^{obs}||_2^2} \tag{2}$$

with $\mathcal{F}_n$ the cost function of the n-th iteration, $E^{obs}(\mathbf{r}_l,\mathbf{r}_m,\omega_k)$ the electric field generated by the actual medium, $E^n(\mathbf{r}_l,\mathbf{r}_m,\omega_k)$ the electric field simulated at the same iteration, N_S the number of transceivers and Ω the set of frequencies involved. These corrections update the parameters as follows $\varepsilon_r^{n+1} = \varepsilon_r^n + \delta\varepsilon_r^n$, $\sigma^{n+1} = \sigma^n + \delta\sigma^n$, and ensure the decay of the cost function between two successive iterations $\mathcal{F}(\varepsilon_r^{n+1},\sigma^{n+1}) < \mathcal{F}(\varepsilon_r^n,\sigma^n)$. They are obtained by solving in the least squares sense the following linear system [12]:

$$E^{obs}(\mathbf{r}_l,\mathbf{r}_m,\omega_k) - E^n(\mathbf{r}_l,\mathbf{r}_m,\omega_k) = \mathrm{j}\,\omega_k\,\varepsilon_0 \times$$
$$\int_{\mathcal{S}} E^n(\mathbf{r},\mathbf{r}_m,\omega_k)\,E^n(\mathbf{r},\mathbf{r}_l,\omega_k)\left(\delta\varepsilon_r^n - \frac{\mathrm{j}\,\delta\sigma^n}{\omega_k\,\varepsilon_0}\right)\mathrm{d}\mathcal{S} \tag{3}$$

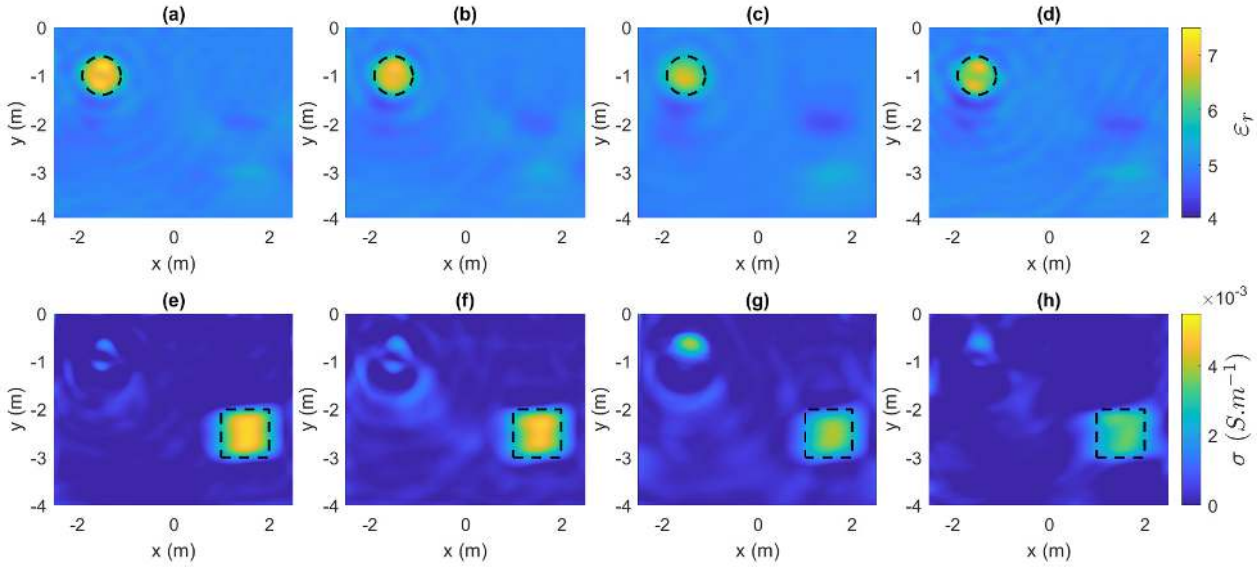

Fig. 2. FWI results of permittivity and conductivity reconstructions by using (a) and (e) *Bunks*, (b) and (f) *Group*, (c) and (g) *Sequential* and (d) and (h) *Simultaneous* strategies

The above integral is computed using the adjoint method and corresponds to the application of the Fréchet derivatives on the parameters corrections. It implies the electric field $E^n(\mathbf{r}, \mathbf{r}_m, \omega_k)$ solution of (1), but also the electric field $E^n(\mathbf{r}, \mathbf{r}_l, \omega_k)$ solution of the adjoint problem, defined by considering the same medium but by positioning the transmitter at $\mathbf{r}_l$.

However, a scaling problem between the variations on conductivity and permittivity can lead to wrong corrections and prevent the algorithm from converging. To overcome this problem, a rescaling parameter called σ_0 is introduced as proposed by [8]. The integral is then split into two contributions. Thus (3) is rewritten in compact form:

$$\delta E(\mathbf{r}_l, \mathbf{r}_m, \omega_k) = \begin{pmatrix} \mathcal{D}_{\varepsilon_r} & \sigma_0 \mathcal{D}_\sigma \end{pmatrix} \begin{pmatrix} \delta\varepsilon_r^n \\ \dfrac{\delta\sigma^n}{\sigma_0} \end{pmatrix} \tag{4}$$

where $\sigma_0 = \varepsilon_0 \omega_k$ if only one frequency is involved, $\sigma_0 = \dfrac{\varepsilon_0}{N_\omega} \sum_{i=1}^{N_\omega} \omega_i$ for N_ω frequencies and $\delta E(\mathbf{r}_l, \mathbf{r}_m, \omega_k) = E^{obs}(\mathbf{r}_l, \mathbf{r}_m, \omega_k) - E^n(\mathbf{r}_l, \mathbf{r}_m, \omega_k)$. Here $\mathcal{D}_{\varepsilon_r}$ and $\mathcal{D}_\sigma$ correspond to the Fréchet derivatives of the cost function with respect to ε_r and σ. Consequently the whole linear system to be solved is formed by concatenating the different Fréchet derivatives taken for each measurement point and for each frequency as well as the differences between the simulated and measured fields. The LSQR algorithm [13] is applied to solve the above linear system. Its number of iterations is fixed at 10 for regularization purpose. The inversion process is driven by a *Matlab* code which repetitively calls upon the software *Comsol Multiphysics*® to manage the forward model part.

B. Frequency strategies

To get an optimal reconstruction, a comparison of 4 strategies involving 8 different frequencies is considered. The choice of the frequencies (25, 30, 40, 50, 75, 100, 125 and 170 MHz) based on [14] avoids the so-called "cycle skipping" phenomenon. These strategies are described as follows :

1) the *Bunks Strategy* consists in using simultaneously frequency packets according to the following sequence [6] : (f_1), (f_1,f_2), ..., (f_1, .. ,f_8). The result of the first packet is used as initialization of the new one.
2) the *Group Strategy* consists in the use of frequencies by packets of two according to the sequence (f_1,f_2), (f_2,f_3), ..., (f_7,f_8). The result of the previous frequency group is used to initialize the new one.
3) the *Sequential Strategy* was proposed by Pratt and Worthington [15] and uses the frequencies one at a time in increasing order. Again, the result of the previous frequency is used as initialization of the new frequency.
4) the *Simultaneous Strategy* uses all available frequencies at once.

The convergence is reached when the difference of the cost function between two iterations becomes smaller than a quantity $C : |\mathcal{F}_n - \mathcal{F}_{n-1}| < C$. Choosing $C = 10^{-4}$ ensures that the cost function does not evolve anymore, which means that all the information has been taken into account.

IV. Numerical results

The medium under consideration is meshed with a 1 cm characteristic length, which leads to around 200,000 unknowns for each parameter. The comparative study of the 4 strategies focuses on the accuracy of reconstruction, the convergence rate and the computation time. The accuracy

of the reconstruction is evaluated by the normalized residual error (NRE) which is written as follows:

$$NRE(\zeta) = \frac{||\zeta^{end} - \zeta^{true}||_2^2}{||\zeta^{start} - \zeta^{true}||_2^2} \quad (5)$$

with $\zeta = (\varepsilon_r$ or $\sigma)$. It corresponds to the average error at the end of the reconstruction normalized by the average error at the starting step. The initialization step of the inversion algorithm involves a perfectly homogeneous medium of permittivity 5 and conductivity zero. The initial error is thus the same for all strategies. With such a medium, the smallest wavelength is given for 170 MHz and is equal to 78 cm. All the results presented in this article were obtained on a computer with 128 GB of RAM and AMD Ryzen Threadripper PRO 3955WX 16-Core CPU.

Fig. 2 shows the different reconstructions for both relative dielectric permittivity (top figures) and electrical conductivity (bottom figures). Each column corresponds to one of the frequency strategies described in Section III.B. To qualitatively appreciate the likelihood of the reconstructions compared to the actual inclusions, we have added the shapes of the latter in dashed black lines. The permittivity reconstructions are satisfactory for the 4 configurations even if the *Bunks Strategy* stands out by the accuracy of the reconstruction, Fig. 2a. The other strategies seem to have more oscillations and blurred objects. Concerning the conductivity reconstructions, the observation is quite different. Indeed, the reconstruction using the *Sequential Strategy* produces conductivity artifacts, so it is not acceptable, see Fig. 2g. The other inversion strategies provide satisfactory results even if, once again, the *Bunks Strategy* stands out for its accuracy.

	Bunks	Group	Sequential	Simultaneous
Time (min)	374	173	**102**	192
Iteration number	58	66	75	**19**
NRE (ε_r)	**0.449**	0.495	0.618	0.571
NRE (σ)	**0.436**	0.52	0.646	0.558

The visual, and thus qualitative, impression provided by Fig. 2 is confirmed by the above summary table. Indeed, the *Bunks Strategy* leads to the lowest NRE for the two physical parameters. However, it is very expensive in computation time. In our situation, a good NRE is less than 0,5. The *Group Strategy* has NRE slightly larger than those of the *Bunks* one but is less expensive in computation time even if it takes a few more iterations to converge. As expected, the *Simultaneous Strategy* yields the lowest number of iterations to converge but suffers from long computation time and poor reconstruction.

V. Conclusion

In this work a regularized Gauss-Newton algorithm was used to invert data at several frequencies. Different frequency strategies have been tested and compared with each other. Numerical results of reconstruction of the actual parameters show that the *Bunks Strategy* gives the best spatial resolution i.e. with the lowest normalized residual errors. Then the *Group Strategy* reconstructs the parameters with a slightly lower resolution, a smaller convergence speed, but with a much shorter computation time. Both strategies show that the full waveform inversion leads to a good reconstruction of the parameters of the two inclusions, letting guess their shapes, although they have a characteristic length equal to the smallest wavelength in the homogeneous medium. As a perspective for this work, we plan to apply this full waveform inversion method on GPR experimental data.

References

[1] D. David, "Ground Penetrating Radar", in *IET Digital Library*, 2004, doi: 10.1049/PBRA015E

[2] J. Nocedal and S. Wright, "Numerical Optimization", in *Springer*, 1999, doi: 10.1007/978-0-387-40065-5

[3] N. Huai et al., "Monte Carlo Stochastic inversion of GPR parameters", in *International Geophysical Conference*, pp. 1001-1004, April 2017, doi: 10.1190/IGC2017-254

[4] J. Feng, L. Yang, H. Wang and Y. Song, "GPR-based Subsurface Object Detection and Reconstruction Using Random Motion and DepthNet", in *arXiv*, 2020

[5] A. Tarantola, "Inversion of seismic reflection data in the acoustic approximation", in *Geophysics*, vol. 49, no. 8, pp. 1259–1266, Aug. 1984.

[6] D. Feng, X. Wang and B. Zhang, "A Frequency-Domain Quasi-Newton-Based Biparameter Synchronous Imaging Scheme for Ground-Penetrating Radar With Applications in Full Waveform Inversion", in *IEEE Transactions on Geoscience and Remote Sensing*, vol. 59, pp. 1949-1966, March 2021, doi: 10.1109/TGRS.2020.3004465.

[7] H. Pinard, "Imagerie électromagnétique 2D par inversion des formes d'ondes complètes : Approche multiparamètres sur cas synthétiques et données réelles", *Sciences de la Terre*. Université Grenoble Alpes, 2017, in French. NNT : 2017GREAU041, tel-01830657f

[8] F. Lavoué, "2D Full waveform inversion of ground penetrating radar data : towards multiparameter imaging from surface data", *Earth Sciences*. Université de Grenoble, 2014, in English. NNT : 2014GRENU050, tel-01551800

[9] Q. Didier, S. Arhab and G. Lefeuve-Mesgouez, "Regularized Gauss-Newton Iterative Scheme Applied to Shallow Subsurface Imaging", in *NSG2021 27th European Meeting of Environmental and Engineering Geophysics*, 2021, doi: 10.3997/2214-4609.202120075

[10] W. Chew, "Waves and fields in inhomogeneous media", in *IEEE Press series on electromagnetic waves*, 1995

[11] A. Wirgin, "The inverse crime", 2004, url: https://hal.archives-ouvertes.fr/hal-00001084/file/invcrim.pdf

[12] S. Arhab, D. Anagnostou, and J. Maminirina, "High-order functional derivatives of the scattered field according to the permittivity-contrast function", in *Wave Motion*, vol. 83, pp. 67-79, 2018, doi: 10.1016/j.wavemoti.2018.07.008

[13] C.C. Paige and M. A. Saunders, "LSQR: An algorithm for sparse linear equations and sparse least squares", in *ACM Transactions on Mathematical Software (TOMS)*, 1982, pp. 43-71.

[14] L. Sirgue and R. Pratt, "Efficient waveform inversion and imaging: A strategy for selecting temporal frequencies", in *GEOPHYSICS*, 2004, pp. 231-248, doi : 10.1190/1.1649391

[15] R. G. Pratt and M. H. Worthington, "Inverse theory applied to multi-source cross-hole tomography. Part 1: Acoustic wave-equation method", in *Geophys. Prospecting*, vol. 38, no. 3, pp. 287–310, Apr. 1990.